Journal of Physics: Condensed Matter

PAPER

The stability and surface termination of hexagonal $LuFeO_3$

To cite this article: Shi Cao *et al* 2015 *J. Phys.: Condens. Matter* **27** 175004

The stability and surface termination of hexagonal $LuFeO_3$

Shi Cao[1], Tula R. Paudel[1], Kishan Sinha[1], Xuanyuan Jiang[1], Wenbin Wang[2], Evgeny Y. Tsymbal[1], Xiaoshan Xu[1], and Peter A. Dowben[1].

[1]*Department of Physics and Astronomy, Nebraska Center for Materials and Nanoscience, University of Nebraska, Lincoln, Nebraska 68588, USA,*

[2]*Department of Physics, Fudan University, Shanghai 200433, China*

Abstract:

The surface termination and the nominal valence states for hexagonal $LuFeO_3$ thin films grown on Al_2O_3(0001) substrates were characterized by angle resolved X-ray photoemission spectroscopy (ARXPS). The Lu 4f, Fe 2p, and O 1s core level spectra indicate that both the surface termination and the nominal valence depend on surface preparation, but the stable surface terminates in a Fe-O layer. This is consistent with the results of density functional calculations which predict that the Fe-O termination of $LuFeO_3$(0001) surface is energetically favorable and stable over a broad range of temperatures and oxygen partial pressures when it is reconstructed to eliminate surface polarity.

Keywords: Lutetium Ferrite, X-ray Photoemission for surface analysis, Density functional theory, Multiferroic/magnetoelectric films, Epitaxial and superlattice films

PACS numbers: 79.60.-i, 71.15.Mb, 74.25.Jb, 77.55.Nv, 77.55.Px

I. Introduction

The hexagonal lutetium ferrite (h-$LuFeO_3$) is an example of one of the few multiferroic materials in which the spontaneous ferroelectric and magnetic ordering simultaneously present at room temperature [1-3]. Ferroelectricity in h-$LuFeO_3$ appears below a T_c = 1050 K, followed by an antiferromagnetic ordering below the Néel temperature of T_N = 440 K. Decreasing the temperature below 130 K, a weak spontaneous ferromagnetic polarization appears along the *c*-axis, due to the Dzyaloshinskii-Moriya and single ion anisotropy mechanism [4,5]. This leads to multiple types of ferroic ordering and novel magnetoeletric coupling [5,6] in the same system. From the point of view of applications, if the magneto-electric coupling is to be exploited in this system, the surface termination and surface stability is of paramount importance. The surface termination affects the polarization of the surface and of the interface with other materials, which will have a significant influence on the voltage control of magnetization for magnetoelectric logic and memory device applications. Yet, the detailed structural and electronic properties at the interface between h-$LuFeO_3$ and the substrates or at the surface (the interface with vacuum) [8] of the $LuFeO_3$ have been given little attention thus far [1-4,6-11].

Here we have investigated the structural and electronic properties of the surface and the stability of h-$LuFeO_3$ using angle-resolved x-ray photoemission spectroscopy (ARXPS), complemented by x-ray diffraction (XRD) and density functional theory (DFT). Given the surface sensitivity due to the short mean free path of the photoelectron, angle resolved XPS has proven to be an effective approach to characterizing the surfaces of complex oxides [12-20], as confirmed by low-energy ion scattering (LEIS) and a host

of other techniques [20]. These ARXPS techniques have been applied to the manganites [12-20], and also apply to the ferrites. From this, based on the Lu 4f, Fe 2p and O 1s core level electronic structure, as well as density functional theory, we are able to show that the favored surface termination of h-$LuFeO_3$ is Fe-O instead of Lu-O_2.

II. Experimental

Hexagonal $LuFeO_3$ films (50 nm) [1,2] were deposited on Al_2O_3 (0001) and yttrium stabilized zirconia (YSZ) (111) substrates using pulsed laser (248 nm) deposition. The depositions were carried out in a 5 mtorr O_2 background gas at 750 ^oC with a laser fluence of 1 J/cm^2. The crystal structures of the h-$LuFeO_3$ films were characterized by x-ray diffraction using a Rigaku D/Max-B diffractometer, with the Co Kα radiation (1.7903 Å).

The angle-resolved X-ray photoemission spectra (ARXPS) were obtained using SPECS PHOIBOS 150 energy analyzer. A non-monochromatized Al Kα x-ray source, with photo energy 1486.6 eV was used with various emission angles, as indicated. The core level binding energies were calibrated on the basis of a gold reference, with Au $4f_{7/2}$ core level peak placed at 84 eV was used to calibrate the system, all at room temperature. Due to the insulating nature of the sample, the charging effects were evident assigning the adventitious C 1s feature to 284.8 eV provided an additional calibration of binding energy. Photoemission take–off angle was adjusted by rotating the manipulator with accuracy ±1°. The CasaXPS software was used to analyze the X-ray photoemission core level spectra [21] and a Shirley-type background was subtracted to obtain X-ray

photoemission core level spectra peak areas [22,23]. The ARXPS experiments were carried out on multiple samples (h-LFO on Al_2O_3 (0001) and/or YSZ substrates) and no significant differences between the XPS core level spectra observed.

III. Computational methods

Theoretical modeling of the h-$LuFeO_3$ films stacking in the (0001) direction (Fig. 1) was performed using density functional theory, the projected augmented wave method [24], and Perdew-Burke-Ernzerhof pseudopotentials [25], as implemented in Vienna *ab initio* simulation package [26]. We fully relaxed the structure with the force convergence limit of |0.03| eV/Å for each atom. Correlation effects beyond generalized gradient approximation (GGA) were treated at a semi-empirical GGA+U level within a rotationally invariant formalism [27] with a U = 5 eV chosen for the Fe 3d-orbitals.

In order to investigate the surface composition, we calculated the surface grand potential of 19 layers thick symmetric 144 atoms Lu-O_2 and 141 atoms Fe-O terminated slabs, so as to avoid creation of a polar field, unless noted otherwise. Two slabs were separated by 15 Å vacuum, to avoid the interaction between them. The in plane lattice constant was taken from experiment [28] and kept fixed while internal coordinate were completely relaxed.

IV. The nominal oxidation state of h-$LuFeO_3$

The surface of hexagonal lutetium ferrite (h-$LuFeO_3$) is fragile with respect to low energy argon ion sputtering, and the surface composition and nominal valence state of the surface and near surface (selvage region) can be modified. The X-ray photoemission spectra for the Fe 2p, O 1s and Lu 4f core levels show significant differences after argon ion sputtering compared to "as grown" (pristine) sample, as seen in Fig. 2. These changes are particularly evident in the Fe 2p satellite photoemission features and Lu 4f shallow core level.

The Fe 2p core level photoemission spectra not only contain the $2p_{3/2}$ and $2p_{1/2}$ but also three satellite peaks (labeled by the dashed lines A, B, and C in Fig. 2a) and excellent signatures of the nominal valence state of the iron in $LuFeO_3$. The peak position of the Fe 2p core level photoemission satellite features have been well studied for Fe^{2+}, Fe^{3+} and mixed valance state compounds [29-34]. In comparing our data with these prior studies, it is clear that for pristine h-$LuFeO_3$ thin films, the Fe 2p and satellite peaks are characteristic of a nominal Fe^{3+} valance, and as the features do not vary with emission angle, both surface and bulk are in the nominal Fe^{3+} valance state. This changes after the sputtering or after the sputtering and annealing (to ~400 K in ultra-high vacuum) combination.

With sputtering, and even with post annealing, the XPS spectra of Fe 2p and associated satellite peaks characteristic of a nominal Fe^{3+} valance develop the signatures of the characteristics of a nominal Fe^{2+} valance, as seen in in Fig. 2a. In the transition from the nominal Fe^{3+} valance to Fe^{2+}, the relative binding energies of the Fe 2p satellite features move to the lower (smaller) binding energies, as do the main 2p core level photoemission features, as noted in prior studies of iron oxides [33,34]. Accompanying

the general shift to lower binding energies, the energy separation between the satellite peaks and the main Fe $2p_{3/2}$ core level photoemission peak also decreases. The XPS satellite peaks (labeled by C in Fig. 2a) move closer, in apparent binding energy, to the Fe $2p_{3/2}$ core level feature. This energy separation between the multiplet features and the main Fe $2p_{3/2}$ and Fe $2p_{1/2}$ features, in XPS, is a signature of a change in the nominal valence of the iron [29-34]. These changes to the core level photoemission spectra indicate that the Fe local environment changes with Ar ion sputtering and annealing, and indeed is expected, since the oxygen deficiencies (oxygen depletion) can occur [33,34]. The electron density around the Fe ion decreases so the binding energies for both the Fe 2p satellite and the main core level peak also decrease.

The experimental XPS Fe $2p_{3/2}$ core level line shape for h-$LuFeO_3$ may be even further fitted with the multiplet peaks of Gupta and Sen [35,36] for both pristine surface of a nominal Fe^{3+} valance and the surface where defects were introduced by Ar^+ ion sputtering and annealed in ultra-high vacuum (UHV). This fitting of the $2p_{3/2}$ envelope by a detailed assignment of multiplets, as applied by Gupta and Sen to high spin Fe^{3+} compound [35,36] is a tertiary indicator of the nominal Fe valance state. If the pristine h-$LuFeO_3$ is entirely Fe^{3+} in the surface region, then the multiplet fitting of Gupta and Sen should be consistent results with other iron compounds [29,30,37]. In the spirit of multiplet fitting of Gupta and Sen [24,35,36], the fittings of the peak positions and intensity contributions to the various multiplets, for the pristine sample, agrees with the expected Fe (III) compound multiplet configuration, as summarized in Fig. 2c with the key fitting parameters listed in table I. The only deviation from expectation is that the photoemission full width at half maximum (FWHM) for the various multiplet features is

slightly larger than the typical values [29,30,37]. Taken as a whole, the multiplet fine structure is a further reliable indicator that the iron of pristine surface is in the nominally pristine Fe^{3+} state. In a similar vein, for the surface following sputtering and annealing treatments, the fittings of the peak positions and intensity contributions to the various multiplets (Fig. 2c) and the fit of the $2p_{3/2}$ envelope (Fig. 3a) must include a Fe^{2+} component to agree with the multiplet fitting of Gupta and Sen (Fig. 2c and Table1).

The iron 2+, introduced by argon ion sputtering and annealing, is a result of defect creation. With more significant sputtering and higher annealing temperatures, the Fe 2p photoemission features peaks show increasingly stronger characteristic signatures of Fe^{2+} (labeled by "Fe^{2+}" dashed line in Fig. 3b). While the characteristic signatures of Fe^{2+} in the photoemission spectra of h-$LuFeO_3$ are increasingly resolvable after annealing at 1000 K, the creation of oxygen vacancies is partially reversible. The intensity of the characteristic signatures of Fe^{2+}, in core level photoemission, decreases after the annealing in 1×10^{-8} torr O_2 environment, as shown in Fig. 3b.

The fragile nature of the h-$LuFeO_3$ stoichiometry is also evident in X-ray diffraction (XRD), as shown in Fig. 3c. After multiple cycles of argon ion sputtering and UHV annealing, additional peaks appear in the XRD spectrum, indicating an impurity phases. The XRD spectrum obtained for a sample annealed in UHV treatment shows evidence of a minority phase (arrow in Fig. 3c) other than h-$LuFeO_3$. This minority phase can be reduced or removed and converted back to the hexagonal phase after annealing in 1 atm O_2 at 600° C (bottom of Fig. 3c). The hexagonal phase, h-$LuFeO_3$, is stable as a thin film on Al_2O_3(0001) substrates [1, 2], but the stable phase for $LuFeO_3$ is orthorhombic phase (o-$LuFeO_3$), not the hexagonal phase. The fact that the hexagonal

phase can be recovered in the sputtered sample after annealing at high oxygen pressure (~1 atm) at ~600 ^{o}C, is indicative that it is the hexagonal phase that is the stable phase of the epitaxial $LuFeO_3$ thin films on Al_2O_3(0001) substrates and that the energy of the Al_2O_3 (0001)/h-$LuFeO_3$ (0001) interface has lower energy than other possible interfaces [2].

V. Surface termination and possible reconstruction of h-$LuFeO_3$

Both density functional theory (DFT) and angle resolved X-ray photoemission (XPS) indicate that the Fe-O surface termination is favored. As noted in the introduction, angle resolved X-ray photoemission spectroscopy (ARXPS) may be used to estimate the surface composition of complex oxides [12-20] by making use of the changes in the effective mean free path of the escaping photoelectron, which decreases with the increasing photoemission take-off angle. The variations in the photoemission Fe $2p_{3/2}$ to Lu 4f intensity ratio is plotted in Fig. 4. With the increasing take-off angle, the intensity ratio for pristine sample increases, indicating the Fe contribution is greater at the surface than Lu ions, suggesting that the surface is terminated by Fe-O instead of Lu-O_2. As the sample is crystalline, forward scattering must be anticipated [12,38-43]. This forward scattering in angle-resolved XPS contributes to the sharp rise in the Fe/Lu ratio at about 11-20° off normal (forward scattering is expected at about 16°).

After moderate argon ion sputtering, the rich Fe-O surface layer is removed and the underlayer exposed leading a Lu-O_2 termination of the surface of h-$LuFeO_3$. This is evident in the angle-resolved XPS data as a reduction of the Fe $2p_{3/2}$ to Lu 4f intensity

ratio with increasing emission angle away from the surface normal, as clearly seen in Fig. 4. We find there is the relationship between the surface termination and the shape of the Lu 4f core level features. For the pristine sample (Fe-O terminated as discussed above), the Lu 4f is split in the photoemission spectra into the $4f_{7/2}$ and $4f_{5/2}$ spin-orbit components, as shown in Fig. 2b.

When the termination of the surface of h-$LuFeO_3$ is Lu-O_2, as a result of argon ion sputtering, the shape of Lu 4f feature changes and the separation of the $4f_{7/2}$ and $4f_{5/2}$ components is almost not resolvable (Fig. 2b). While the valency of the Lu 4f may not change, the local environment of Lu does, leading to a surface and bulk component for both the $4f_{7/2}$ and $4f_{5/2}$ [44-46]. There are the complications as while the electronic structure of a rare earth 4f state is generally regarded as a core level [47-48], and often thought not affected by the valence electron and/or crystal field, the rare earth 4f peaks lie close to Fermi level and seen to be part of the valence band [46,49-53] thus strongly influenced by the valence band and changes of crystal field. The changes to the Lu $4f_{7/2}$ (8.5 eV) and $4f_{5/2}$ (7.1 eV) XPS shallow core levels, in this latter context, are not surprising at all and consistent with prior work [46,52].

The Fe-O surface termination evident in angle-resolved photoemission is consistent with the predictions of our DFT calculations. To investigate the surface composition, we calculated the surface grand potential for symmetric Lu-O_2 and Fe-O terminated slabs. The surface grand potential G_S [54] is defined as $Gs = \frac{1}{2A}\left(E_s - (N_{Lu}\mu_{Lu} + N_{Fe}\mu_{Fe} + N_O\mu_o)\right)$, where A is the surface area, and chemical potentials (μ's) are defined with respect to those of the Lu and Fe solids and

molecular O (*i.e.* $\mu = \mu_{el} + \Delta\mu$) and calculated assuming that the surface is in thermodynamic equilibrium with bulk. Using $\mu_O^{el} = \frac{1}{2}E(O_2) = 4.66$ eV, and the experimental Lu_2O_3 formation enthalpy [55] ($H_f = E(Lu_2O_3) - 2\mu_{Lu}^{el} + 3\mu_O^{el}$), we determined μ^{el}_{Lu}. Similarly using the experimental Fe_2O_3, FeO and Fe_3O_4 formation energies [55] we determined μ^{el}_{Fe}. Using the relationships $3\Delta\mu_O + \Delta\mu_{Lu} + \Delta\mu_{Fe} = H_f\ (LuFeO_3)$, with a calculated value of -14.17 eV/mol, for the formation energy of $LuFeO_3$ and taking into account that $3\Delta\mu_O + 2\Delta\mu_{Lu} \leq H_f(Lu_2O_3)$ and $3\Delta\mu_O + 2\Delta\mu_{Fe} \leq H_f(Fe_2O_3)$ to avoid the formation of Lu_2O_3 and Fe_2O_3, and $\Delta\mu_O$, $\Delta\mu_{Fe}$ and $\Delta\mu_{Lu} \leq 0$ to avoid formation of elemental Lu, Fe and O_2, we determined the region of the chemical potentials where $LuFeO_3$ is stable. This is displayed in Fig. 5b, where the shaded area of stable $LuFeO_3$ is bounded by formation of Fe_2O_3 and Lu_2O_3. At each point inside this region of stable $LuFeO_3$, we calculated the surface grand potential for the Lu-O_2 and Fe-O surfaces. The regions where the Lu-O_2 and Fe-O surface terminations have the lowest grand potential are shaded in red and blue respectively in Fig. 5a. The oxygen chemical potential can be converted to temperature and pressure using the relation $\Delta\mu_O(T, P) = (H_0+c_p(T-T_0)-TS_0+Tc_p ln(T/T_0) + k_B T ln(P/P_0))/2$ derived using the ideal gas law, where $c_p=3.5k_b$, $k_b = 1.4\times10^{-23}\ m^2kgs^{-2}K^{-1}$ and tabulated values for oxygen at $T_0 = 298\ K$ and $P_0=1\ atm$ are $H_0=8700\ Jmol^{-1}$ and $S_0=205\ Jmol^{-1}K^{-1}$. It can be seen from Fig. 5a that except for lower oxidizing conditions, the Fe-O surface is unstable. The above consideration, however, does not take into account the tendency for the polar surfaces to reconstruct.

The fact that both Lu-O_2 and Fe-O pristine surface terminations are charged means that they are unstable and thus highly susceptible to surface reconstructions.

Theoretically, we consider a simple surface reconstruction that leads to a charge neutral surface. The (2x1) Fe-O surface with one iron vacancy ((2x1) Fe-O+V(1Fe)), and the (2x2) Lu-O_2 surface with three oxygen vacancies (2x2 Lu-O_2+V(3O)) are expected to be neutral based on their polar charges. Following the method described above we calculated the grand potential for the reconstructed surfaces and plotted the surface phase stability diagrams in Fig. 5c and 5d. It is evident that contrary to the results for the unreconstructed pristine surface, the Fe-O surface termination is stable over a broad range of temperatures and oxygen partial pressures (Fig. 5c). In oxidizing/Fe poor conditions, formation of Fe vacancies is facile and a defective Fe-O surface is stable, whereas in reducing/Fe rich conditions Fe vacancy formation is energetically unfavorable and the unreconstructed Fe-O surface is stable. This means that the energy gain by polarity reduction in this case is smaller than that required to form Fe vacancy. The grand potential of (2x2) Lu-O_2+V(3O) is higher than (1x1) Fe-O even in O poor area, and hence (1x1) Fe-O surface remains more stable. Thus, overall stability phase diagram now is covered by Fe-O surfaces—(2x1) Fe-O+V(1Fe) in the Fe poor/O rich conditions and (1x1) Fe-O surface in Fe rich/O poor conditions.

VI. Conclusion

We find in all our experimental studies that the h-$LuFeO_3$ (0001) basal face surface terminates in Fe-O, consistent with density functional theory calculations. The polar Fe-O surface is seen to be susceptible to reconstructions and vacancy formation, again in both experiment and theory, and this effect is much more dramatic under high temperature and

ultrahigh vacuum (UHV). The stability of the h-$LuFeO_3$ phase for films on Al_2O_3 (0001) substrates is further confirmed by the fact that the impurity phase generated by sputtering and annealing in UHV can be converted back to the hexagonal phase.

Acknowledgements

This project was supported by the National Science Foundation through the Nebraska MRSEC (Grant No. DMR-1420645) and by the Semiconductor Research Corporation through the Center for Nanoferroic Devices, an SRC-NRI Center under Task ID 2398.001. X.S Xu acknowledges the support from Nebraska EPSCoR.

References

[1] W B Wang, J Zhao, W Wang, Z Gai, N Balke, M Chi, H N Lee, Wei Tian, L Zhu, X Cheng, D J Keavney, J Yi, T Z Ward, P C Snijders, H M Christen, W Wu, Jian Shen and X Xu 2013 *Phys. Rev. Lett.* **110** 237601

[2] X Xu and W B Wang 2014 *Mod. Phys. Lett.* B **28** 1430008

[3] H Das, A L Wysocki, Y N Geng, W D Wu and C J Fennie 2014 *Nature Commun*. **5** 2998

[4] A R Akbashev, A S Semisalova, N S Perov and A R Kaul 2011 *Appl. Phys. Lett.* **99** 122502

[5] I Dzyaloshinsky 1958 *J. Phys. and Chem. Solids* **4** 241

[6] A Masuno, S Sakai, Y Arai, H Tomioka, F Otsubo, H Inoue, C Moriyoshi, Y Kuroiwa and J D Yu 2009 *Ferroelectrics* **378** 169

[7] W B Wang, H Wang, X Xu, L Zhu, L He, E Wills, X Cheng, D J Keavney, J Shen, X Wu and X Xu 2012 *Appl. Phys. Lett.* **101** 241907

[8] A R Akbashev, V V Roddatis, A L Vasiliev, S Lopatin, V A Amelichev and A R Kaul 2012 *Sci. Repts.* **2** 672

[9] J A Moyer, R Misra, J A Mundy, C M Brooks, J T Heron, D A Muller, D G Schlom and P Schiffer 2014 *Appl. Phys. Lett. Materials* **2** 012106

[10] H W Wang, I V Solovyev, W Wang, X Wang, P J Ryan, D J Keavney, J-W Kim, T Z Ward, L Zhu, J Shen, X M Cheng, L He, X Xu and X Wu 2014 *Phys. Rev.* B **90** 014436

[11] V V Pavlov, A R Akbashev, A M Kalashnikova, V A Rusakov, A R Kaul, M Bayer, R V Pisarev 2012 *J. Applied Physics* **111**, 056105.

[12] J Choi, J Zhang, S-H Liou, P A Dowben and E W Plummer 1999 *Phys. Rev.* B **59** 13453

[13] H Dulli, E W Plummer, P A Dowben, J Choi and S-H Liou 2000 *Appl. Phys. Lett.* **77** 570

[14] H Dulli, P A Dowben, S-H Liou and E W Plummer 2000 *Phys. Rev.* B **62** R14629

[15] C N Borca, D Ristoiu, Q L Xu, S-H Liou, S Adenwalla and P A Dowben 2000 *J. Appl. Phys.* **87** 6104

[16] C N Borca, Bo Xu, T Komesu, H-k Jeong, M T Liu, S-H Liou and P A Dowben 2002 *Surf. Sci. Lett.* **512** L346

[17] H Jalili, J W Han, Y Kuru, Z Cai and B Yildiz 2011 *J. Phys. Chem. Lett.* **2** 801

[18] R Bertacco, J P Contour, A Barthelemy and J Olivier 2002 *Surf. Sci.* **511** 366

[19] R Cheng, B Xu, C N Borca, A Sokolov, C-S Yang, L Yuan, S-H Liou, B Doudin and P A Dowben 2001 *Appl. Phys. Lett.* **79** 3122-3124

[20] L Poggini, S Ninova, P Graziosi, M Mannini, V Lanzilotto, B Cortigiani, L Malavolti, F Borgatti, U Bardi, F Totti, I Bergenti, V A Dediu and R Sessoli 2014 *J. Phys. Chem.*C **118** 13631

[21] CasaXPS Version 2.3.1 1999

[22] M Repoux 1992 *Surf. Interface Anal.* **18** 567

[23] D A Shirley 1972 *Phys. Rev.* B **5** 4709

[24] P E Blöchl 1994 *Phys. Rev.* B **50** 17953

[25] J P Perdew, K Burke and M Ernzerhof 1996 *Phys. Rev. Lett.* **77** 3865

[26] G Kresse and J Furthmüller 1996 *Phys. Rev.* B **54** 11169

[27] S L Dudarev, G A Botton, S Y Savrasov, C J Humphreys and A P Sutton 1998 *Phys. Rev.* B **57** 1505

[28] E Magome, C Moriyoshi, Y Kuroiwa, A Masuno and H Inoue 2010 Jpn. J. Appl. Phys. **49** 09ME06

[29] A P Grosvenor, B A Kobe, M C Biesinger and N S McIntyre 2004 *Surf. Interface Anal.* **36** 1564

[30] N S McIntyre and D G Zetaruk 1977 *Anal. Chem.* **49** 1521

[31] T Yamashita and P Hayes 2008 *Appl. Surf. Sci.* **254** 2441

[32] P C J Graat and M A J Somers 1996 *Appl. Surf. Sci.* **100** 36

[33] J P Coad and J G Cunningham 1974 *J. Electron Spectros. Related Phenomena* **3** 435

[34] T C Lin, G Seshadri and J A Kelber 1997 *Appl. Surf. Sci.* **119** 83

[35] R P Gupta and S K Sen 1974 *Phys. Rev.* B **10** 71

[36] R P Gupta and S K Sen 1975 *Phys. Rev.* B **12** 15

[37] M C Biesinger, B P Payne, A P Grosvenor, L W M Lau, A R Gerson and R S Smart 2011 *Appl. Surf. Sci.* **257** 2717

[38] W F Egelhoff Jr 1984 *Phys. Rev.* B **30** 1052

[39] W F Egelhoff Jr 1987 *Phys. Rev. Lett.* **59** 559

[40] R A Armstrong and W F Egelhoff Jr 1985 *Surf. Sci.* **154** L225

[41] W F Egelhoff Jr 1989 *J. Vac. Sci. Technol.* A **7** 2060

[42] B Lépine, A Quémerais, D Sébilleau, G Jézéquel, D Agliz, Y Ballini and A Guivarc'h 1994 *J. Appl. Phys.* **76** 5218

[43] H K Jeong, T Komesu, Cheol-Soo Yang, P A Dowben, B D Schultz and C J Palmstrøm 2004 *Mater. Lett.* **58** 2993

[44] D Spanjaard, C Guillot, M-C Desjonqueres, G Treglia and J Lecante 1985 *Surf. Sci. Rep.* **5** 1

[45] D Li, J Zhang, P A Dowben and K Garrison 1993 *J. Phys.: Condens. Matter* **5** L73

[46] Ya B Losovyj, D Wooten, J Colón Santana, J M An, K D Belashchenko, N Lozova, J Petrosky, A Sokolov, J Tang, W Wang, N Arulsamy and P A Dowben 2009 *J. Phys.: Condens. Matter* **21** 045602

[47] B N Harmon and A J Freeman 1974 *Phys. Rev.* B **10** 1979

[48] P A Dowben, D N McIlroy and Dongqi Li 1997 *Surface Magnetism of the Lanthanides*, *Handbook on the Physics and Chemistry of Rare Earths,* Edited by K A Gschneidner and LeRoy Eyring (North Holland Press vol. **24** chapter 159 1-46)

[49] D M Bylander and L Kleinman 1994 *Phys. Rev.* B **49** 1608

[50] J Morrison, D M Bylander and L Kleinman 1993 *Phys. Rev. Lett.* **71** 1083

[51] D M Bylander and L Kleinman 1994 *Phys. Rev.* B **50** 1363

[52] I N Yakovkin, C Waldfried, Takashi Komesu and P A Dowben 2002 *Phys. Lett.* A **304** 43

[53] T Komesu, H-K Jeong, J Choi, C N Borca, P A Dowben, A G Petukhov, B D Schultz and C J Palmstrøm 2003 *Phys. Rev.* B **67** 035104

[54] F Bottin, F Finocchi and C Noguera 2003 *Phys. Rev.* B **68** 035418

[55] D Wagman 1982 *The NBS Tables of Chemical Thermodynamic Properties: Selected Values for Inorganic and C and C Organic Substances in SI Units* (American Chemical Society and the American Institute of Physics for the National Bureau of Standards, New York, Washington, DC).

Figure Captions:

Figure 1 (color online) Unit cell of h-$LuFeO_3$ showing the charged Fe-O and Lu-O_2 layers.

Figure 2 (color online): The core level electron structure of h-$LuFeO_3$ for pristine (both at 0° and 60° take-off angle), sputtered-only and sputtered and annealed samples taken at 0° take-off angle. (a) Fe 2p peaks with three satellite peaks labeled by A, B and C. (b) Lu 4f and O 1s core lines. (c) the Gupta and Sen (GS) multiplets fittings for Fe $2p_{3/2}$ peaks with Shirley background indicated. The four multiplets from Fe^{3+} and three multiplets from Fe^{2+} were shown by bolded (magenta) line and (blue) dot respectively. The (green) dash line indicates the possible surface contribution. The fitting parameters were labeled in Table I. Binding energies are in terms of $E_F - E$.

Figure 3 (color online): (a) Comparisons of XPS Fe $2p_{3/2}$ spectra for pristine h-$LuFeO_3$ sample taken at 0° (black line), 60° (green line) take-off angles with respect to the surface normal and sputtered and annealed sample taken at 0° with respect to the surface normal (blue line) illustrating the broadening at around 709 eV where the signature of Fe^{2+} may exist in the spectra. (b) The shape and peak intensity changes in the Fe 2p spectra after intensive sputtering and annealing cycles (see text), but the spectra were taken at room temperature. The dash line Fe^{2+} shows the Fe^{2+} components. (c) Recovery of the hexagonal phase indicated by XRD in the UHV treated sample after annealing in 1

atmosphere oxygen. The arrow indicates an impurity peak. Binding energies are in terms of $E_F - E$.

Figure 4 (color online): The XPS intensity (peak area) ratio of Fe $2p_{3/2}$ core level relative to the Lu 4f (the latter containing both $4f_{7/2}$ and $4f_{5/2}$ components), as a function of photoemission take-off angle with respect to the surface normal. The dash lines are just meant as guide lines. (a) The (black) triangle and (red) spot shows the variation of the peak area ratios with take-off angle indicating Fe-O and Lu-O_2 surface termination for a pristine and sputtered surface respectively. (b) The XPS intensity (peak area) ratio of Fe $2p_{3/2}$ core level relative to the Lu 4f, an indication of a Fe-O termination for a separate sample.

Figure 5 (color online): Results of theoretical calculations of the h-$LuFeO_3$ (0001) surface phase stability. Partial pressure (pO_2)-temperature plot showing the stability conditions for the unreconstructed (1x1) Lu-O_2 and (1x1) Fe-O polar surfaces (a) and the reconstructed (2x1) Fe-O+V(1Fe) and (1x1) Fe-O non-polar surfaces (c); and their chemical potential representation of plot in (b) and (d) respectively.

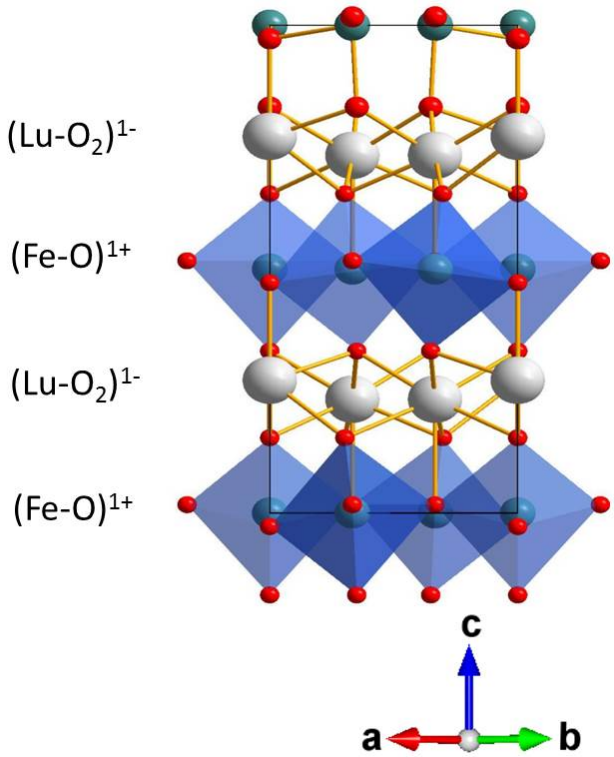

Figure 1.

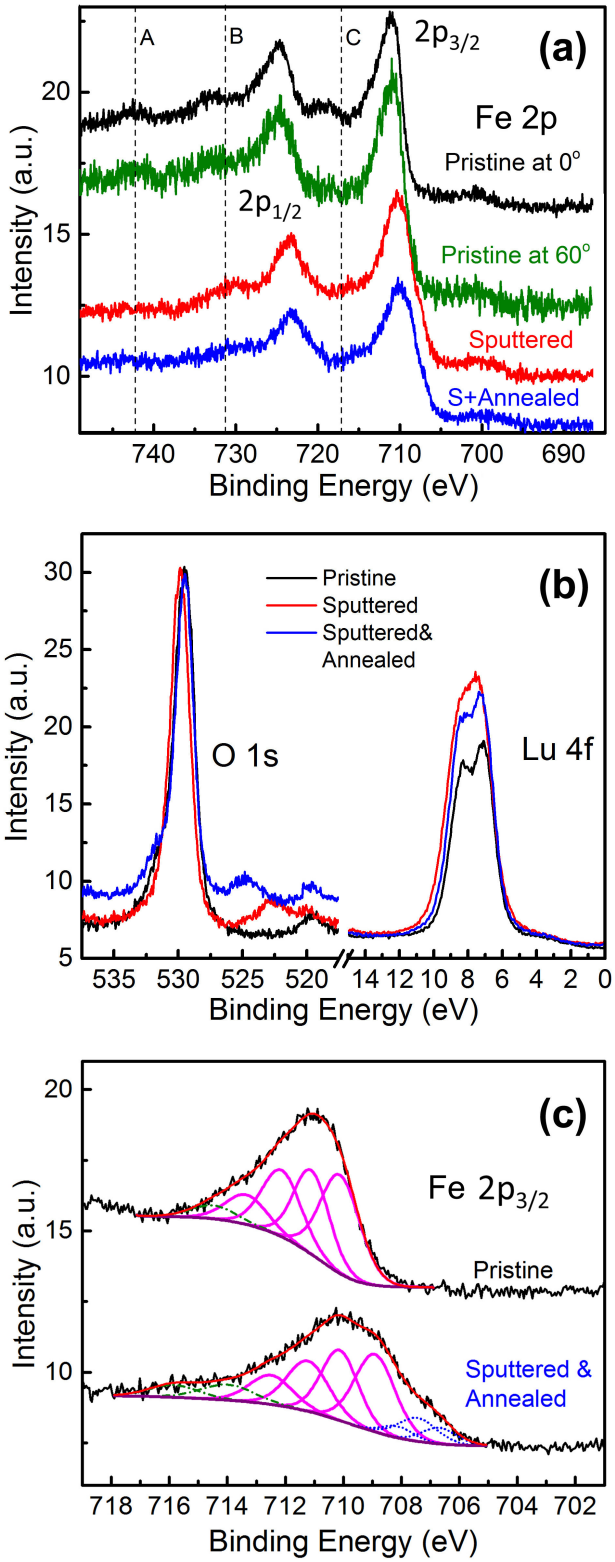
(a)
A
B
C
2p3/2
2p1/2
Fe 2p
Pristine at 0°
Pristine at 60°
Sputtered
S+Annealed
Intensity (a.u.)
Binding Energy (eV)
(b)
Pristine
Sputtered
Sputtered& Annealed
O 1s
Lu 4f
Intensity (a.u.)
Binding Energy (eV)
(c)
Fe 2p3/2
Pristine
Sputtered & Annealed
Intensity (a.u.)
Binding Energy (eV)

Figure 2.

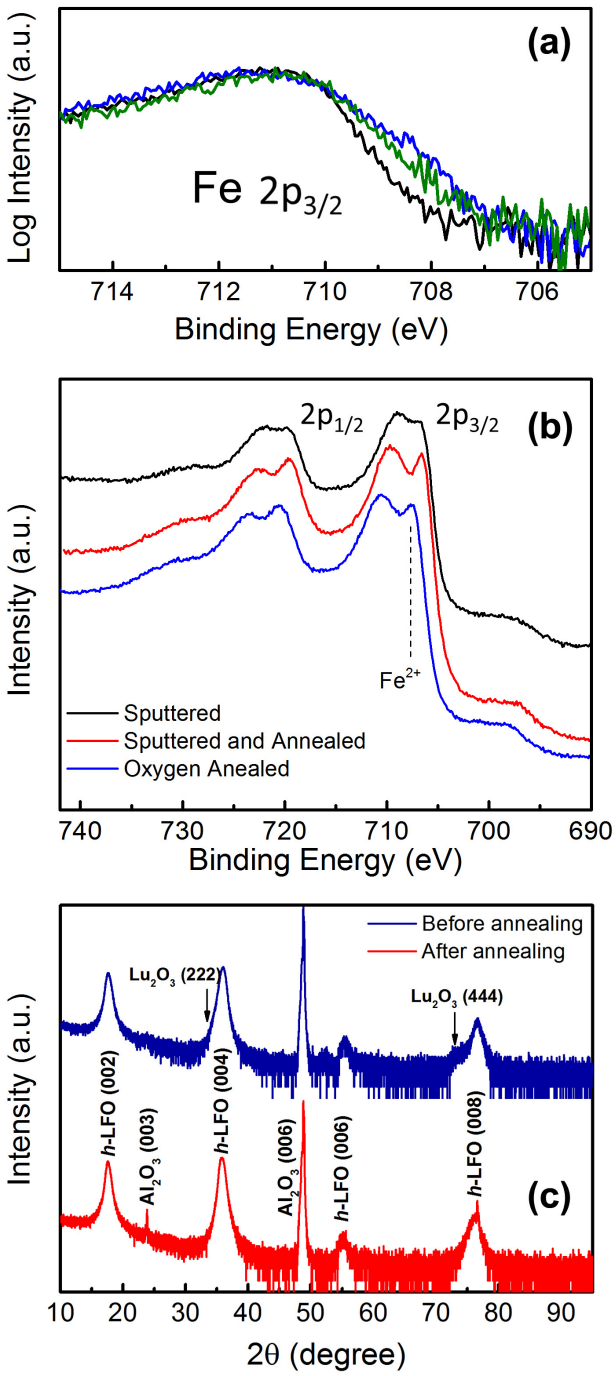
(a)
Log Intensity (a.u.)
Fe 2p3/2
714
712
710
708
706
Binding Energy (eV)
(b)
2p1/2
2p3/2
Intensity (a.u.)
Fe2+
Sputtered
Sputtered and Annealed
Oxygen Anealed
740
730
720
710
700
690
Binding Energy (eV)
(c)
Before annealing
After annealing
Lu2O3 (222)
Lu2O3 (444)
h-LFO (002)
Al2O3 (003)
h-LFO (004)
Al2O3 (006)
h-LFO (006)
h-LFO (008)
Intensity (a.u.)
10
20
30
40
50
60
70
80
90
2θ (degree)

Figure 3.

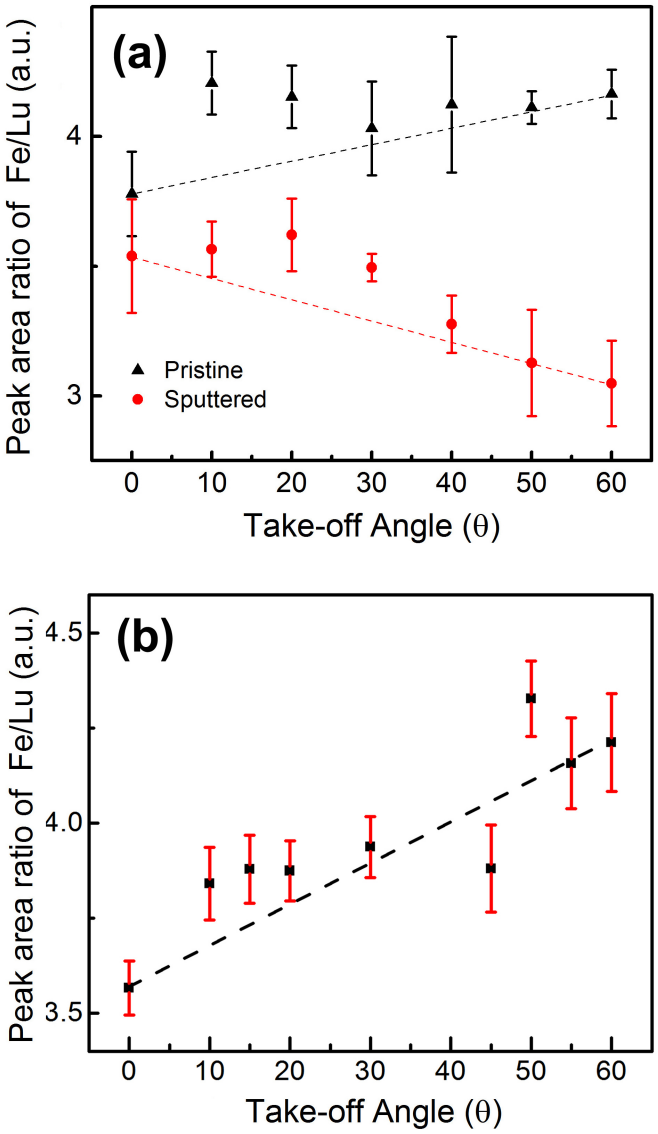
(a)
Peak area ratio of Fe/Lu (a.u.)
4
3
Pristine
Sputtered
0
10
20
30
40
50
60
Take-off Angle (θ)
(b)
Peak area ratio of Fe/Lu (a.u.)
4.5
4.0
3.5
0
10
20
30
40
50
60
Take-off Angle (θ)

Figure 4.

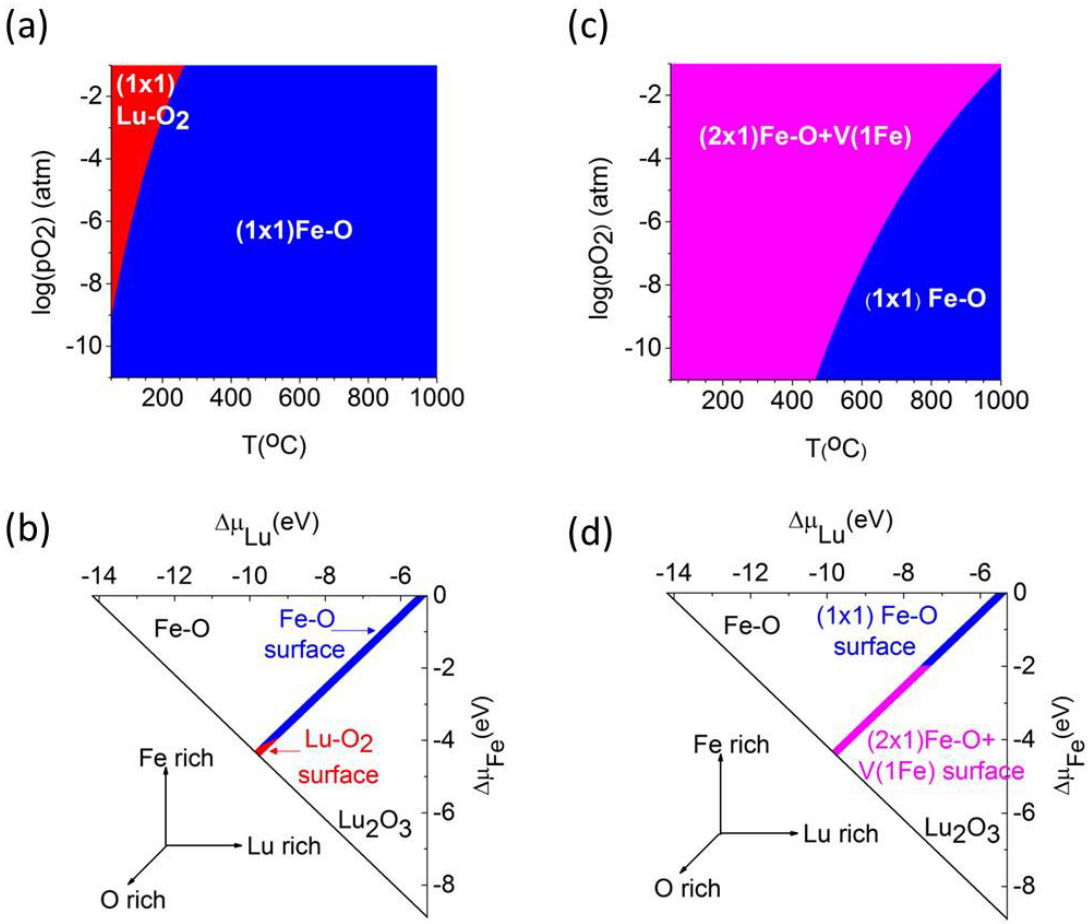
(a)
(1x1)
Lu-O2
(1x1)Fe-O
log(pO2) (atm)
T(°C)
(c)
(2x1)Fe-O+V(1Fe)
(1x1) Fe-O
log(pO2) (atm)
T(°C)
(b)
Δμ_Lu(eV)
Fe-O
Fe-O surface
Lu-O2 surface
Fe rich
Lu rich
O rich
Lu2O3
Δμ_Fe(eV)
(d)
Δμ_Lu(eV)
Fe-O
(1x1) Fe-O surface
(2x1)Fe-O+ V(1Fe) surface
Fe rich
Lu rich
O rich
Lu2O3
Δμ_Fe(eV)

Figure 5.

TABLE I. Comparison of the Gupta and Sen (GS) multiplet peak parameters (Fe $2p_{3/2}$) used to fit the Fe^{3+} and Fe^{2+} nominal valence core level spectra obtained in the compound h-$LuFeO_3$ (h-LFO) and other Fe (III, II) compounds.

Compound	Peak 1 (eV) [FWHM]	%	Peak 2 (eV) [FWHM]	%	ΔE (eV) (Peak2-Peak1)	Peak 3 (eV) [FWHM]	%	ΔE (eV) (Peak3-Peak2)	Peak 4 (eV) [FWHM]	%	ΔE (eV) (Peak4-Peak3)	Ref.
h-LFO(Fe^{3+})[a]	710.1[1.6[d]]	36.4	711.1[1.4]	27.8	1.0	712.2[1.6]	24.4	1.1	713.4[1.7]	11.4	1.2	This work
h-LFO(Fe^{3+})[b]	708.9[1.6]	34.4	710.1[1.5[d]]	28.5	1.2	711.2[1.7]	23.2	1.1	712.5[1.7]	13.8	1.3	This work
Ave. Fe_2O_3[c]	709.8[1.1]	33.2	710.8[1.0]	30.6	1.0	711.6[0.8]	23.4	0.8	712.7[1.1]	12.9	1.1	[37]
Fe^{3+} GS multiplets		39.9		30.4	1.6		19.6	1.3		10.1	0.6	[36,29]
h-LFO(Fe^{2+})[b]	706.7[1.4[d]]	30.3	707.5[1.6]	49.5	0.8	708.1[1.3[d]]	20.1	0.6				This work
FeO	708.4[1.4]	35.2	709.7[1.6]	43.7	1.3	710.9[1.6]	21.1	1.2				[29]
Fe^{2+} GS multiplets		36.1		46.4	1.4		17.5	1.6				[36,29]

[a] The pristine sample which means as grown without any sputtering or annealing treatment.

[b] Sample was sputtered and annealed and then Fe^{2+} peaks shown. The ratios for Fe^{2+} and Fe^{3+} were normalized to the corresponding GS multiplets, which means, for Fe^{3+} the area sum of peak1-4 was 100% and for Fe^{2+} the area sum of peak1-3 was 100%.

[c] In the original reference, the ratio was calculated for GS multiplets and also satellites. For the comparison, the area ratio was normalized for peak 1-4, the GS multiplets only.

[d] The full width at haft maximum was constrained to the bolded number and the reset was obtained by fitting.